Preprint Title Tunable superconducting neurons for networks based on radial basis functions

Authors Andrey E. Schegolev, Nikolay V. Klenov, Sergey V. Bakurskiy, Igor I. Soloviev, Mikhail Y. Kupriyanov, Maxim V. Tereshonok and Anatoli S. Sidorenko

Publication Date 17 März 2022

Article Type Full Research Paper

ORCID® iDs Nikolay V. Klenov - https://orcid.org/0000-0001-6265-3670; Mikhail Y. Kupriyanov - https://orcid.org/0000-0003-1204-9664

Tunable superconducting neurons for networks based on radial basis functions

Andrey E. Schegolev[1,2], Nikolay V. Klenov*[3,4], Sergey V. Bakurskiy[1,5], Igor I. Soloviev[1,4], Mikhail Yu. Kupriyanov[1], Maxim V. Tereshonok[2] and Anatoli S. Sidorenko[6,7]

Address: [1]Skobeltsyn Institute of Nuclear Physics, Lomonosov Moscow State University, Moscow, 119991, Russia; [2]Moscow Technical University of Communication and Informatics (MTUCI), 111024 Moscow, Russia; [3]Faculty of Physics, Lomonosov Moscow State University, Moscow, 119991, Russia; [4]Lobachevsky State University of Nizhni Novgorod Faculty of Physics, 603950 Nizhny Novgorod, Russia; [5]Dukhov All-Russia Research Institute of Automatics, Moscow 101000, Russia; [6]Institute of Electronic Engineering and Nanotechnologies ASM, MD2028 Kishinev, Moldova and [7]Laboratory of Functional Nanostructures, Orel State University named after I.S. Turgenev, 302026, Orel, Russia

Email: Nikolay V. Klenov - nvklenov@gmail.com

* Corresponding author

Abstract

The hardware implementation of signal microprocessors based on superconducting technologies seems relevant for a number of niche tasks where performance and energy efficiency are critically important. In this paper, we consider the basic elements for superconducting neural networks on radial basis functions (RBF). We examine the static and dynamic activation functions of the proposed neuron. Special attention is paid to tuning of the activation functions to the Gaussian form with relatively large amplitude. We proposed and investigated heterostructures designed for the implementation of tunable inductors which consist of superconducting, ferromagnetic, and normal layers.

Keywords

superconducting electronics; Josephson circuits; spintronics; superconducting neural network; networks on radial-basis functions

Introduction

For modern telecommunications, probabilistic identification of various sources in a broadband group signal is extremely important. Also, the probabilistic analysis is used in the consideration of stochastic processes [1-4], as a popular machine learning method for spatial interpolation of non-stationary and non-Gaussian data [5], as a central part of compensation block to enhance the tracking performance in control systems for a class of nonlinear and non-Gaussian stochastic dynamic processes [6].

An important example for this work is the cognitive radio, which is able to receive information about the features of the "radio-environment" and adjust its operating parameters based on this data [7-13]. Similar problems arise nowadays when reading data in superconducting noisy intermediate-scale quantum (NISQ) computers [14-17]. Here again, we need real-time identification and classification of varying signals from multiple sources (qubits) in a narrow frequency range. When working with large data, it's necessary to create specialized neural networks at the hardware level to effectively solve such problems.

Josephson digital circuits and analog receivers have been used for a long time to create software-defined radio-systems [18-25] as well as read-out circuits for quantum computing [26-33]. They realize a unique combination of a wide dynamic range and high sensitivity when receiving signals, with high-performance and energy efficiency at the stage of the processing. It seems reasonable to implement additional processing of incoming data inside the cryo-system using the capabilities of neural network computing [34-43]. The creation of extremely low-dissipating element base for such systems is a very actual scientific and technical task that requires theoretical and experimental studies of the features of macroscopic quantum interference in the complex Josephson circuits.

The direct use of the previously proposed superconducting adiabatic neural network (ANN) based on the perceptron [44-48] for probabilistic identification is not possible. In particular, during the formation of the output signal in the ANN, the so-called global approximation of the input signal is implemented [11,12], in which almost all neurons are included in signal processing. In addition, the perceptron is a fully connected network, which means an abundance of synaptic connections between neurons. These circumstances supposes a highly resource-intensive learning of the network for signal analysis. There is an alternative approach with a representation of the input set of data into the set of output values by using only one hidden layer of neurons. Each of these neurons is responsible for its own area of the parameter space of incoming data. This is the probabilistic or Bayesian approach, where radial-basis functions (for example, Gaussian-like functions) are used as neuron activation functions.

The most common networks operating on this principle are radial basis function networks (RBFN) (also known as Bayesian networks). When using such a network, objects are classified on the basis of assessments of their proximity to neighboring samples. For each sample, a decision can be made based on the selection of the most likely class from those to which the sample could belong. Such a solution requires an estimate of the probability density function for each class. This score is obtained by consideration of training data. The formal rule is that the class with the tightest distribution in the scope of the unknown instance will take precedence over other classes. The traditional approach for estimating the probability density for each class is to assume that the density has some definite form. The normal distribution is the most preferred since it allows one to estimate such parameters of the model as the mean and standard deviation analytically. The superconducting implementation of the key elements of the discussed neural networks is the focus of this work.

Results and Discussion

Model of tunable Gauss-neuron: numerical simulations

A usual architecture of the considered RBFN [49] is presented in figure 1a. These networks have only one hidden layer of neurons on which components of the input vector x are fed. Every neuron of the hidden layer calculates the values of the 1D function $h_k(x)$.

$$h_k(\vec{x}) = exp\left\{-\frac{(\|x - x_k\|)^2}{2\sigma_k^2}\right\}, \tag{1}$$

where x_k is a k^{th} reference point, σ_k – scattering parameter for one-dimensional function $h_k(\vec{x})$.

In this paper, we propose a modified tunable neuron circuit [44] for RBFN (see figure 1b), with a Gaussian-like activation function. It consists of two identical Josephson junctions JJ_1 and JJ_2 in the shoulders with input inductances, L, and output inductunce L_{out}. It is also used to set an additional bias magnetic flux, Φ_b. Flux biasing is used to provide a suitable transfer function for asynchronous circulation of currents in the connected circuits. We will further call such a cell a *Gauss-neuron* or a *G-cell/neuron*.

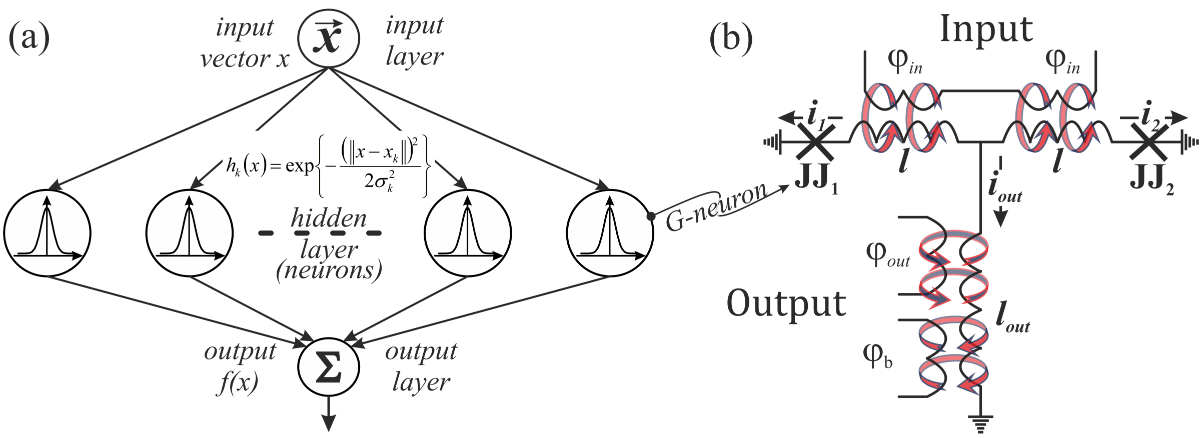

Figure 1: (a) Schematic illustration of a RBF-network. (b) Schematic representation of a Gauss-neuron ensured Gauss-like transfer function.

Hereinafter we use normalized values for typical parameters of the circuit: all fluxes (input Φ_{in} and output Φ_{out}, bias Φ_b) are normalized to the flux quantum Φ_0; currents are normalized to the critical current of the Josephson junctions I_C; inductances are normalized to the characteristic inductance $2\pi L I_C/\Phi_0$, times are normalised to the characteristic time $t_C = \Phi_0/(2\pi V_C)$ (V_C is a characteristic voltage of a Josephson junction). Equations of motion were obtained in terms of half-sum and half-difference of Josephson phases φ_1, φ_2 ($\theta = (\varphi_1 + \varphi_2)/2$ and $\psi = (\varphi_1 - \varphi_2)/2$):

$$\dot{\theta} = \frac{\varphi_b - \theta}{l + 2l_{out}} - \sin\theta\cos\psi, \tag{2}$$

$$\dot{\psi} = -\frac{\varphi_{in} + \psi}{l} - \sin\psi\cos\theta. \tag{3}$$

The output magnetic flux obeys the following equation:

$$\varphi_{out} = \frac{2l_{out}}{l + 2l_{out}} \cdot (\theta - \varphi_b)\,. \tag{4}$$

Figure 2(a,b) below shows the families of transfer functions of a Gauss-neuron at different bias fluxes. They are compared with the radial-basis function taken in the form $g(x) = exp(-x^2/(2\sigma^2))$ (dashed line). All transfer functions were normalized to normalized to their maximum value, since at the first stage we were interested in the shape of the curve itself. It can be seen that the shape of the response meets the requirements; in addition, it can be adjusted using a bias magnetic flux φ_b. An important feature of the system is that it also allows non-volatile tuning with memory using tunable inductances l and l_{out}, see figure 2(c-e). Estimations for different values of φ_b show that the best match (with Gauss-like radial-basis function) can be achieved with $\varphi_b = 0.05\pi$ and inductance values $l = 0.1$, $l_{out} = 0.1$. Also the investigation of the full width at half maximum (FWHM) and the amplitude of the transfer functions of the Gauss-neuron was carried out for different values of φ_b (figure 2(c-d)) and inductance l (figure 2(e)). It can be seen that an increase in the value of the inductance l decreases FWHM of the transfer function and increases its amplitude. The bias flux is a convenient adjustment of transfer function of the tunable Gauss-neuron; bias flux should vary in the $[0...0.5]\pi$ range to save the proper form of the transfer function. The mean of the transfer function can be controlled by an additional constant component in the input flux. By selecting the parameters of a configurable G-neuron, we can make the effective field period for the activation function large enough for practical use in the real neural networks (figure 2(e)).

We calculated the standard deviation (SD) of the transfer function from the Gaussian-like function $g(x)$ with fixed amplitude. The obtained results are presented in the $\{l, l_{out}\}$ plane. This visualization

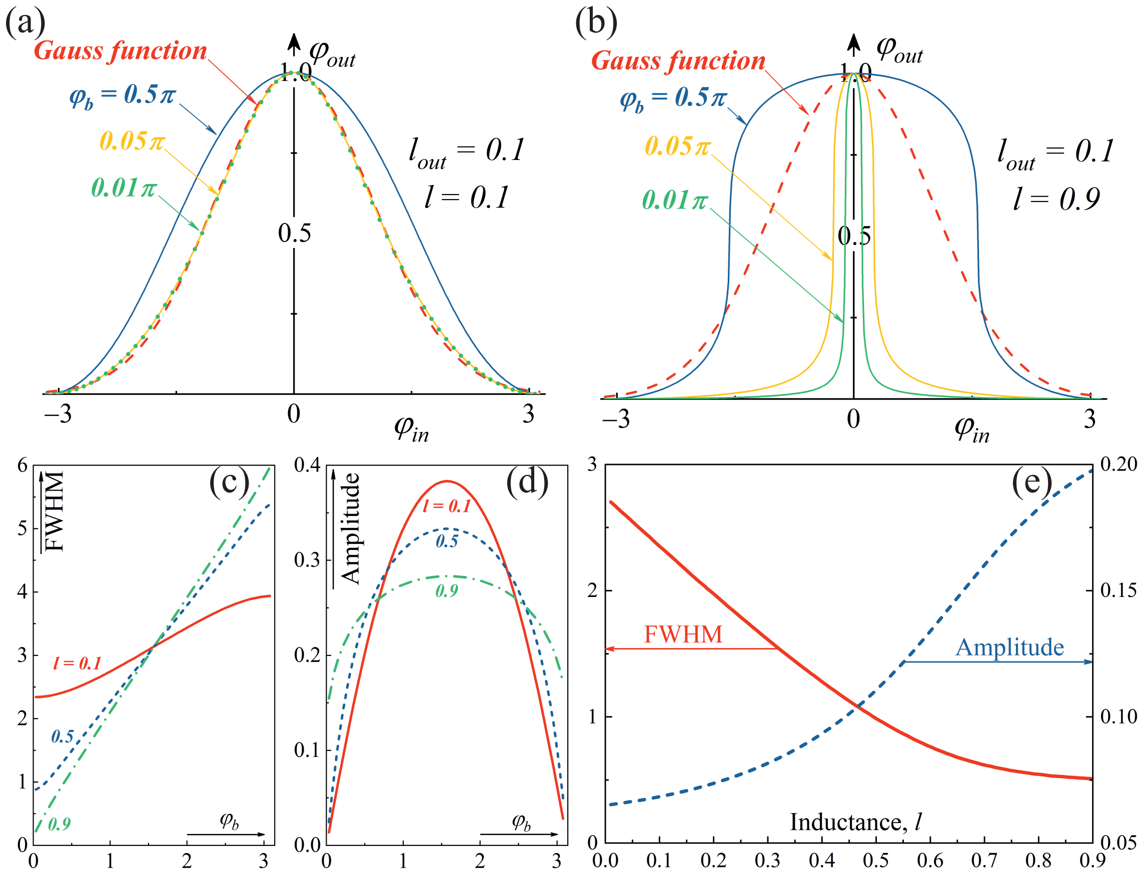

Figure 2: Transfer functions (normalised) and its main characteristics for the Gauss-neuron. (a), (b) Families of the normalised transfer functions depending on the magnitude of the bias flux φ_b for various pairs of inductances l and l_{out}: (a) $l = 0.1$, $l_{out} = 0.1$; (b) $l = 0.9$, $l_{out} = 0.1$. (c) Dependencies of *full width at half maximum* (FWHM) and *amplitude* on the bias flux φ_b of transfer functions for $l = 0.1, 0.5, 0.9$ with $l_{out} = 0.1$. d) Dependencies of *FWHM* and *amplitude* on the inductance l for transfer functions of the Gauss-neuron at $l_{out} = 0.1$ and $\varphi_b = 0.05 \cdot \pi$.

allows to find the most proper operating parameters for the considered element. The magnitude of the amplitude of the transfer function was also presented (Figures 3(a,b)). The optimal values of inductance corresponding to the minimum of SD lies in the hollow of the surface, see figure 3(b). The minimum SD value is reached at $l = 0.1$, $l_{out} = 0.1$. The position of the hollow in figure 3(b) could be expressed as $(l_{out})_{SD} \approx 0.8 - 0.55 \cdot (l)_{SD}$. At the same time, for relatively small φ_b the transfer function amplitude increases with increase of the output and shoulder inductunces, l_{out} and l. Thus, the choice between the proximity of the transfer function to a Gaussian-like form and the maximization of the response amplitude is determined by the specifics of the network when solving a specific problem. Once again, we emphasize: variations in the parameters of the circuit within a fairly wide range allows one to change the amplitude and width of the activation function, while maintaining its Gaussian-like shape.

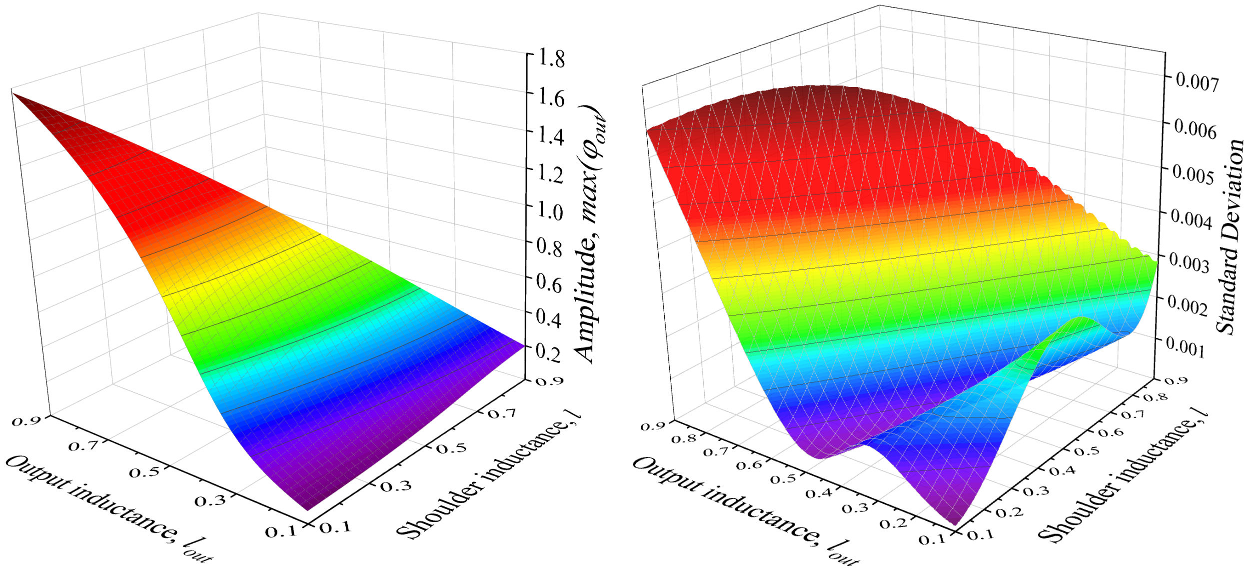

a) b)

Figure 3: Amplitude of the transfer function (a) and its standard deviation from the Gaussian-like function (b) depending on the inductances l and l_{out} of the G-cell. Bias flux is equal to 0.05π.

The dynamic transfer functions of the system were also calculated (figure 4(a)). The input magnetic signal is a smoothed trapezoidal function of time with rise/fall time t_{RF}, see the insert in the figure 4(b). It can be seen that the dynamic activation function of the required type without hysteresis can be obtained with adiabatic operation of the cell (t_{RF} up to $8000 t_C$, where t_C is the characteristic time for the Josephson junction).

Realization of tunability: adjustable kinetic inductance

For neural networks based on the considered G-neurons, tunable linear elements (inductors) with memory properties are extremely important. This allows the *in situ* switching between operating modes directly on the chip. The tunable passive devices are usually based on thin superconducting strips, which demonstrate non-linear properties of kinetic inductance at a large current comparable to the critical one [50,51]. Perspective types of controllable devices consist on the hybrid structures

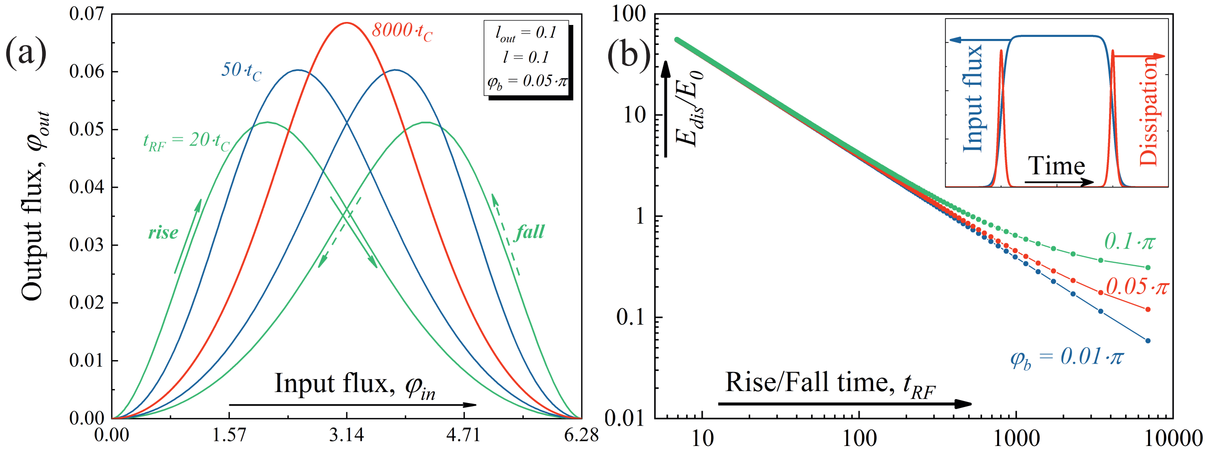

Figure 4: (a) Dynamic transfer function of a Gauss-neuron for a trapezoidal external signal for different values of the rise / fall times of the signal t_{RF} and (b) Energy dissipation, normalised to the characteristic energy $E_0 = \Phi_0 I_C / 2\pi$, by rise-fall time of the input signal for different bias fluxes: $\varphi_b = \{0.01, 0.05, 0.1\} \cdot \pi$. Insert demonstrates the form of temporal dynamic for input flux and dissipation. If the critical current for Josephson junctions I_C is equal to $100\mu A$ and $\varphi_b = 0.05\pi$ than $E_{dis} \approx 0.01\ aJ$ for $t_{RF} = 6\ ns$ (corresponds to $\approx 1700 \cdot t_C$).

with semiconductors tunable by gate-voltage [52] or include magnetic layers with different possible magnetic states [53] .

A relatively simple way to create the required passive element with non-volatile memory is a tunable kinetic inductance [46] with integrated spin-valve structure. The typical spin-valve [54-56] is a hybrid structure containing at least a pair of ferromagnetic FM-layers with different coercive forces. Variations in the relative orientation of their magnetizations change the distribution of the order parameter, that leads to a noticeable change in the kinetic inductance of the layers. The usage of a thin superconducting spacer (s) between FM layers supports superconducting order parameter and increase efficiency of spin-valve effect [57]. In this article, we propose a development of this approach, allowing to significantly increase the effective variations in the kinetic inductance.

We study proximity effect and electronic transport in the multi-layer hybrid structures in the frame of Usadel equations [58]

$$\pi T_C \xi^2 \left(G \frac{d^2 F}{dx^2} - F \frac{d^2 G_p}{dx^2} \right) - \widetilde{\omega} F = -G\Delta, \qquad G_\omega^2 + F_\omega F_{-\omega}^* = 1; \tag{5}$$

$$\Delta \ln \frac{T}{T_C} + \pi T \sum_{\omega=-\infty}^{\infty} \left(\frac{\Delta}{|\omega|} - F \right) = 0, \tag{6}$$

with Kupriyanov-Lukichev boundary conditions [59]

$$\gamma_B \xi_l \left(\frac{dF_l}{dx} - \frac{F_l}{G_l} \frac{dG_l}{dx} \right) = F_r - F_l \frac{G_r}{G_l} \tag{7}$$

at the S/FM interfaces. Here G and F are normal and anomalous Green's functions, $\omega = \pi T(2n+1)$ is Matsubara frequency. $\widetilde{\omega} = \omega + iH$, where H is the exchange energy (H=0 in S and N layers), l/r – indexes, which denotes the materials from the left and right side from interface, ξ – the coherence length, ρ – resistivity, $\gamma_B = \frac{R_B A}{\rho_l \xi_l}$ – interface parameter, where $R_B A$ – the resistance per square of the interface.

The calculated distribution of the anomalous Green function, F, permits to estimate the ability to influence the propagation of the superconducting correlations (screening properties) for the hybrid structure. The spatial distribution of the screening length directly depends on the proximization of the superconducting order parameter in the system [60]:

$$\lambda(x)^{-2} = \frac{16\pi T^2}{\rho} \sum_{\omega>0}^{Re} \left(F(x)^2 \right). \tag{8}$$

Hence, the screening length and kinetic inductance of the considered s-layers are significantly larger for the parallel orientation of the magnetizations in FM- layers (parallel case) in comparison with the anti-parallel case. It leads to redistribution of the current flowing along the multilayer and increase the total kinetic inductance of the structure [61,62]

$$L_K = \frac{\mu_0 X}{W} \left[\int_0^d \lambda(x)^{-2} dx \right]^{-1} \tag{9}$$

where X is the length of the strip, W – width, and d is the thickness of the multilayer. It can be concluded that small changes in temperature or applied magnetic field [46,63] can significantly change (from zero to relatively large values) the kinetic inductance of thin s-layers in the hybrid structures under consideration. In our calculations, we assume that the currents flowing through the system are weak and do not have the effect of coupling, and the structure itself is much thinner than the screening length of the magnetic flux.

We propose a hybrid structure effectively consisting of three parts: a pairing source, a spin valve, and a low inductive current carrier. The pairing source is a superconductor layer slightly thicker than the critical value at which the self-consistency potential appears. This condition usually corresponds to thicknesses of the order of $(2...3)\ \xi$. The spin valve is a multilayer structure $(FM)_1 - s - (FM)_2 - s - (FM)_1 - s - (FM)_2$ with several ferromagnetic layers $(FM)_1$ and $(FM)_2$ of different thicknesses, separated by thin spacers of a superconductor or normal metal. Remagnetization of the structure by fields of different amplitudes changes the relative orientations of the magnetizations between $(FM)_1$ and $(FM)_2$ layers, which leads to a change of the effective exchange field of the multilayer. This effect can change the efficiency of the Cooper pairs penetration through the multilayer in several times. The current carrier is organized on the basis of a thin strip of low-resistance normal metal, which ensures its lower kinetic inductance relative to the rest of the structure, which leads to the flow of current precisely through this layer.

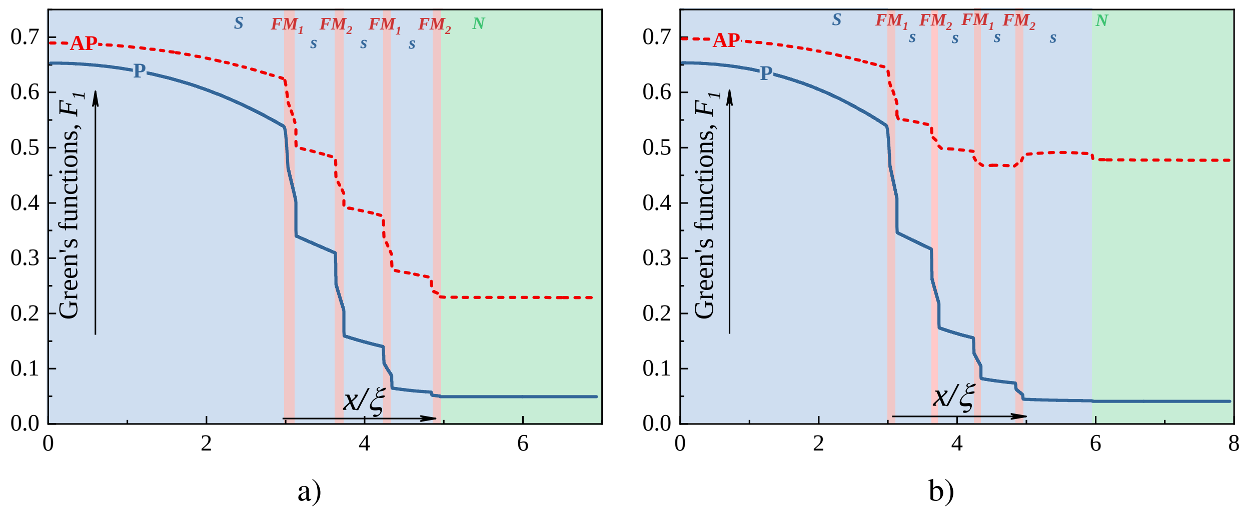

Figure 5: Spatial distribution of the pair amplitude in the hybrid structure a) $S - (FM)_1 - s - (FM)_2 - s - (FM)_1 - s - (FM)_2 - N$ without additional s1-layer and b) $S - (FM)_1 - s - (FM)_2 - s - (FM)_1 - s - (FM)_2 - s_1 - N$ with additional superconducting layer for parallel (blue solid line) and anti-parallel (red dashed line) mutual orientations of magnetization between FM_1 and FM_2 layers.

Figure 5 shows the spatial distributions of the pairing amplitude over a similar structure for parallel and anti-parallel orientations of the magnetization of the FM_1- and FM_2-layers. To enhance the effect, this element can contain an additional superconductor layer s_1 with a thickness less than the critical thickness. In the case of a closed valve, such a structure is in the normal state, and the superconducting correlations in the N-layer are negligible. If the valve is open, the s_1 layer goes over into a superconducting state leading to increase of the amplitude of pair correlations in the N-layer. The spatial distribution of the pairing amplitude in a structure with an additional layer s_1 with similar parameters is shown in the figure 5(b).

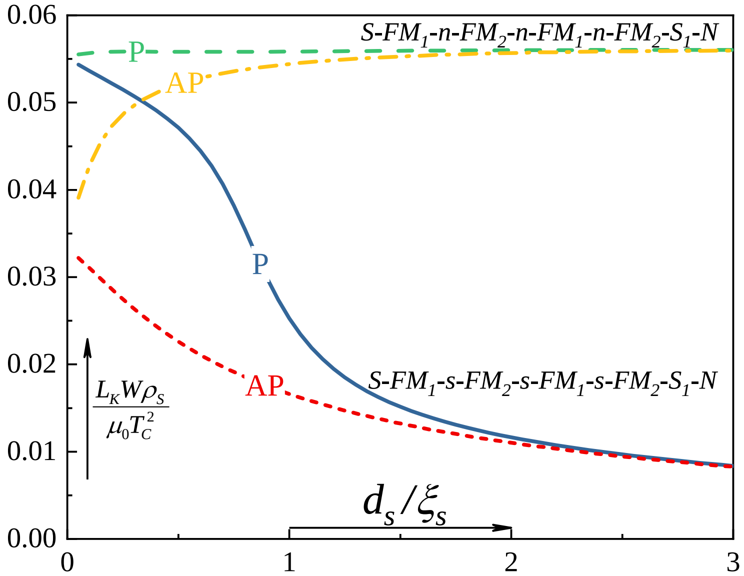

Figure 6: Kinetic inductance of the hybrid structures $S-(FM)_1-s-(FM)_2-s-(FM)_1-s-(FM)_2-s-N$ and $S-(FM)_1-n-(FM)_2-n-(FM)_1-n-(FM)_2-s_1-N$ for parallel (dark blue solid line and long-dashed green line) and antiparallel (red dashed line and orange dash-dot line) mutual orientations of magnetization between FM_1 and FM_2 layers as functions of spacer thickness.

Figure 6 demonstrates the dependence of the kinetic inductance on the thickness of the intermediate $s-$ or n-layers, which determine the efficiency of the spin valve. At large thicknesses of intermediate layers, the valve loses efficiency. In the case of normal spacers, the transition occurs to a completely normal state, where the kinetic inductance of the entire structure coincides with the kinetic inductance of the source layer S. With a large thickness of superconducting spacers s, the valve system also loses efficiency, transferring the entire structure to a completely superconducting state. However, at thicknesses of the order of $(0.5...1)\ \xi$, the maximum spin-valve effect appears, and the total kinetic inductance of the structure changes several times during the switch between states with parallel and antiparallel magnetization orientations.

Conclusion

We have considered a basic cell for superconducting signal neuro-computers designed for fast processing of a group signal with extremely low energy dissipation. It turned out that for this purpose it is possible to modify the previously discussed element of adiabatic superconducting neural networks. The ability to adjust the parameters of the studied Gauss-cell (with Gaussian-like activation function) is very important for *in situ* switching between operating modes. Using microscopic modeling, we have shown that the desired compact tunable passive element can be implemented in the form of a controllable kinetic inductance. An example is a multilayer structure consisting of a superconducting "source", a current-carrying layer and a spin valve with at least two magnetic layers with different thicknesses. The proposed tunable inductance does not require suppression of superconductivity in the source layer. In this case, the spin-gate effect determines the efficiency of penetration of superconducting correlations into the current-carrying layer, which is the reason for the change in inductance.

Acknowledgements

G-neuron and tunable inductance were developed with the support of the Russian Science Foundation (project no. 20-69-47013). The numerical simulations were supported within the framework of the strategic academic leadership program of UNN.

References

1. Turchetti, C.; Crippa, P.; Pirani, M.; Biagetti, G. *IEEE transactions on neural networks* **2008**, *19* (6), 1033–1060.

2. Groth, C.; Costa, E.; Biancolini, M. E. *Aircraft Engineering and Aerospace Technology* **2019**.

3. Zhang, J.; Li, H.; Hu, B.; Min, Y.; Chen, Q.; Hou, G.; Huang, C. Modelling of SFR for Wind-Thermal Power Systems via Improved RBF Neural Networks. In *Chinese Intelligent Systems Conference*; 2020; pp 630–640.

4. Xie, S.; Xie, Y.; Huang, T.; Gui, W.; Yang, C. *IEEE Transactions on Industrial Electronics* **2018**, *66* (2), 1192–1202.

5. Shi, C.; Wang, Y. *Geoscience Frontiers* **2021**, *12* (1), 339–350.

6. Zhou, Y.; Wang, A.; Zhou, P.; Wang, H.; Chai, T. *Automatica* **2020**, *112*, 108693.

7. Abidi, A. A. *IEEE Journal of Solid-State Circuits* **2007**, *42* (5), 954–966. doi:10.1109/JSSC.2007.894307.

8. Ulversoy, T. *IEEE Communications Surveys & Tutorials* **2010**, *12* (4), 531–550.

9. Wang, B.; Liu, K. R. *IEEE Journal of Selected Topics in Signal Processing* **2011**, *5* (1), 5–23. doi:10.1109/JSTSP.2010.2093210.

10. Macedo, D. F.; Guedes, D.; Vieira, L. F. M.; Vieira, M. A. M.; Nogueira, M. *IEEE Communications Surveys Tutorials* **2015**, *17* (2), 1102–1125. doi:10.1109/COMST.2015.2402617.

11. Adjemov, S.; Klenov, N.; Tereshonok, M.; Chirov, D. *Moscow University Physics Bulletin* **2015**, *70* (6), 448–456.

12. Adjemov, S.; Klenov, N. V.; Tereshonok, M.; Chirov, D. *Programming and Computer Software* **2016**, *42* (3), 121–128.

13. Ahmad, W. S. H. M. W.; Radzi, N. A. M.; Samidi, F. S.; Ismail, A.; Abdullah, F.; Jamaludin, M. Z.; Zakaria, M. N. *IEEE Access* **2020**, *8*, 14460–14488. doi:10.1109/ACCESS.2020.2966271.

14. Córcoles, A. D.; Magesan, E.; Srinivasan, S. J.; Cross, A. W.; Steffen, M.; Gambetta, J. M.; Chow, J. M. *Nat. Comm.* **2015**, *6* (1), 1–10.

15. Arute, F.; Arya, K.; Babbush, R.; Bacon, D.; Bardin, J. C.; Barends, R.; Biswas, R.; Boixo, S.; Brandao, F. G.; Buell, D. A. et al. *Nature* **2019**, *574* (7779), 505–510.

16. Babukhin, D. V.; Zhukov, A. A.; Pogosov, W. V. *Phys. Rev. A* **2020**, *101* (5), 052337.

17. Vozhakov, V.; Bastrakova, M. V.; Klenov, N.; Soloviev, I.; Pogosov, W. V.; Babukhin, D. V.; Zhukov, A. A.; Satanin, A. M. *Physics–Uspekhi* **2022**.

18. Fujimaki, A.; Katayama, M.; Hayakawa, H.; Ogawa, A. *Superconductor Science and Technology* **1999**, *12* (11), 708–710. doi:10.1088/0953-2048/12/11/305.

19. Fujimaki, A.; Nakazono, K.; Hasegawa, H.; Sato, T.; Akahori, A.; Takeuchi, N.; Furuta, F.; Katayama, M.; Hayakawa, H. *IEEE Transactions on Applied Superconductivity* **2001**, *11* (1), 318–321. doi:10.1109/77.919347.

20. Brock, D. K.; Mukhanov, O. A.; Rosa, J. *IEEE Communications magazine* **2001**, *39* (2), 174–179.

21. Vernik, I. V.; Kirichenko, D. E.; Filippov, T. V.; Talalaevskii, A.; Sahu, A.; Inamdar, A.; Kirichenko, A. F.; Gupta, D.; Mukhanov, O. A. *IEEE Transactions on Applied Superconductivity* **2007**, *17* (2), 442–445. doi:10.1109/TASC.2007.898613.

22. Gupta, D.; Filippov, T. V.; Kirichenko, A. F.; Kirichenko, D. E.; Vernik, I. V.; Sahu, A.; Sarwana, S.; Shevchenko, P.; Talalaevskii, A.; Mukhanov, O. A. *IEEE Transactions on Applied Superconductivity* **2007**, *17* (2), 430–437. doi:10.1109/TASC.2007.898255.

23. Gupta, D.; Kirichenko, D. E.; Dotsenko, V. V.; Miller, R.; Sarwana, S.; Talalaevskii, A.; Delmas, J.; Webber, R. J.; Govorkov, S.; Kirichenko, A. F.; Vernik, I. V.; Tang, J. *IEEE Transactions on Applied Superconductivity* **2011**, *21* (3), 883–890. doi:10.1109/TASC.2010.2095399.

24. Kornev, V. K.; Soloviev, I. I.; Sharafiev, A. V.; Klenov, N. V.; Mukhanov, O. A. *IEEE Transactions on Applied Superconductivity* **2013**, *23* (3), 1800405–1800405. doi:10.1109/TASC.2012.2232691.

25. Mukhanov, O.; Prokopenko, G.; Romanofsky, R. *IEEE Microwave Magazine* **2014**, *15* (6), 57–65. doi:10.1109/MMM.2014.2332421.

26. Pankratov, A. L.; Gordeeva, A. V.; Kuzmin, L. S. *Phys. Rev. Lett.* **2012**, *109*, 087003. doi:10.1103/PhysRevLett.109.087003.

27. Soloviev, I. I.; Klenov, N. V.; Pankratov, A. L.; Il'ichev, E.; Kuzmin, L. S. *Phys. Rev. E* **2013**, *87*, 060901. doi:10.1103/PhysRevE.87.060901.

28. Soloviev, I. I.; Klenov, N. V.; Bakurskiy, S. V.; Pankratov, A. L.; Kuzmin, L. S. *Applied Physics Letters* **2014**, *105* (20), 202602. doi:10.1063/1.4902327.

29. Soloviev, I. I.; Klenov, N. V.; Pankratov, A. L.; Revin, L. S.; Il'ichev, E.; Kuzmin, L. S. *Phys. Rev. B* **2015**, *92*, 014516. doi:10.1103/PhysRevB.92.014516.

30. McDermott, R.; Vavilov, M. G.; Plourde, B. L. T.; Wilhelm, F. K.; Liebermann, P. J.; Mukhanov, O. A.; Ohki, T. A. *Quantum Science and Technology* **2018**, *3* (2), 024004. doi:10.1088/2058-9565/aaa3a0.

31. Opremcak, A.; Pechenezhskiy, I. V.; Howington, C.; Christensen, B. G.; Beck, M. A.; Leonard, E.; Suttle, J.; Wilen, C.; Nesterov, K. N.; Ribeill, G. J.; Thorbeck, T.; Schlenker, F.; Vavilov, M. G.; Plourde, B. L. T.; McDermott, R. *Science* **2018**, *361* (6408), 1239–1242. doi:10.1126/science.aat4625.

32. Howington, C.; Opremcak, A.; McDermott, R.; Kirichenko, A.; Mukhanov, O. A.; Plourde, B. L. T. *IEEE Transactions on Applied Superconductivity* **2019**, *29* (5), 1–5. doi:10.1109/TASC.2019.2908884.

33. Leonard, E.; Beck, M. A.; Nelson, J.; Christensen, B.; Thorbeck, T.; Howington, C.; Opremcak, A.; Pechenezhskiy, I.; Dodge, K.; Dupuis, N.; Hutchings, M.; Ku, J.; Schlenker, F.; Suttle, J.; Wilen, C.; Zhu, S.; Vavilov, M.; Plourde, B.; McDermott, R. *Phys. Rev. Applied* **2019**, *11*, 014009. doi:10.1103/PhysRevApplied.11.014009.

34. Chiarello, F.; Carelli, P.; Castellano, M. G.; Torrioli, G. *Superconductor Science and Technology* **2013**, *26* (12), 125009. doi:10.1088/0953-2048/26/12/125009.

35. Segall, K.; LeGro, M.; Kaplan, S.; Svitelskiy, O.; Khadka, S.; Crotty, P.; Schult, D. *Phys. Rev. E* **2017**, *95*, 032220. doi:10.1103/PhysRevE.95.032220.

36. Schneider, M. L.; Donnelly, C. A.; Russek, S. E.; Baek, B.; Pufall, M. R.; Hopkins, P. F.; Dresselhaus, P. D.; Benz, S. P.; Rippard, W. H. *Science Advances* **2018**, *4* (1), e1701329. doi:10.1126/sciadv.1701329.

37. Shainline, J. M.; Buckley, S. M.; McCaughan, A. N.; Chiles, J.; Jafari-Salim, A.; Mirin, R. P.; Nam, S. W. *Journal of Applied Physics* **2018**, *124* (15), 152130. doi:10.1063/1.5038031.

38. Shainline, J. M.; Buckley, S. M.; McCaughan, A. N.; Chiles, J. T.; Jafari Salim, A.; Castellanos-Beltran, M.; Donnelly, C. A.; Schneider, M. L.; Mirin, R. P.; Nam, S. W. *Journal of Applied Physics* **2019**, *126* (4), 044902. doi:10.1063/1.5096403.

39. Cheng, R.; Goteti, U. S.; Hamilton, M. C. *IEEE Transactions on Applied Superconductivity* **2019**, *29* (5), 1–5. doi:10.1109/TASC.2019.2892111.

40. Toomey, E.; Segall, K.; Berggren, K. K. *Frontiers in neuroscience* **2019**, 933.

41. Toomey, E.; Segall, K.; Castellani, M.; Colangelo, M.; Lynch, N.; Berggren, K. K. *Nano Letters* **2020**, *20* (11), 8059–8066. doi:10.1021/acs.nanolett.0c03057. PMID: 32965119

42. Ishida, K.; Byun, I.; Nagaoka, I.; Fukumitsu, K.; Tanaka, M.; Kawakami, S.; Tanimoto, T.; Ono, T.; Kim, J.; Inoue, K. *IEEE Micro* **2021**, *41* (03), 19–26. doi:10.1109/MM.2021.3070488.

43. Feldhoff, F.; Toepfer, H. *IEEE Transactions on Applied Superconductivity* **2021**, *31* (5), 1–5. doi:10.1109/TASC.2021.3063212.

44. Schegolev, A. E.; Klenov, N. V.; Soloviev, I. I.; Tereshonok, M. V. *Beilstein journal of nanotechnology* **2016**, *7* (1), 1397–1403.

45. Soloviev, I. I.; Schegolev, A. E.; Klenov, N. V.; Bakurskiy, S. V.; Kupriyanov, M. Y.; Tereshonok, M. V.; Shadrin, A. V.; Stolyarov, V. S.; Golubov, A. A. *Journal of applied physics* **2018**, *124* (15), 152113.

46. Bakurskiy, S.; Kupriyanov, M.; Klenov, N. V.; Soloviev, I.; Schegolev, A.; Morari, R.; Khaydukov, Y.; Sidorenko, A. S. *Beilstein journal of nanotechnology* **2020**, *11* (1), 1336–1345.

47. Schegolev, A.; Klenov, N.; Soloviev, I.; Tereshonok, M. *Superconductor Science and Technology* **2021**, *34* (1), 015006.

48. Schneider, M.; Toomey, E.; Rowlands, G. E.; Shainline, J.; Tschirhart, P.; Segall, K. *Superconductor Science and Technology* **2022**.

49. Park, J.; Sandberg, I. W. *Neural computation* **1991**, *3* (2), 246–257.

50. Annunziata, A. J.; Santavicca, D. F.; Frunzio, L.; Catelani, G.; Rooks, M. J.; Frydman, A.; Prober, D. E. *Nanotechnology* **2010**, *21* (44), 445202.

51. Bockstiegel, C.; Wang, Y.; Vissers, M.; Wei, L.; Chaudhuri, S.; Hubmayr, J.; Gao, J. *Applied physics letters* **2016**, *108* (22), 222604.

52. Splitthoff, L. J.; Bargerbos, A.; Grünhaupt, L.; Pita-Vidal, M.; Wesdorp, J. J.; Liu, Y.; Kou, A.; Andersen, C. K.; van Heck, B. *arXiv preprint arXiv:2202.08729* **2022**.

53. Jué, E.; Iankevich, G.; Reisinger, T.; Hahn, H.; Provenzano, V.; Pufall, M. R.; Haygood, I. W.; Rippard, W. H.; Schneider, M. L. *Journal of Applied Physics* **2022**, *131* (7), 073902.

54. Fominov, Y. V.; Golubov, A. A.; Karminskaya, T. Y.; Kupriyanov, M. Y.; Deminov, R. G.; Tagirov, L. R. *JETP Lett.* **2010**, No. 6, 308.

55. Leksin, P.; Garif'Yanov, N.; Garifullin, I.; Fominov, Y. V.; Schumann, J.; Krupskaya, Y.; Kataev, V.; Schmidt, O.; Büchner, B. *Physical review letters* **2012**, *109* (5), 057005.

56. Lenk, D.; Morari, R.; Zdravkov, V. I.; Ullrich, A.; Khaydukov, Y.; Obermeier, G.; Müller, C.; Sidorenko, A. S.; von Nidda, H.-A. K.; Horn, S.; Tagirov, L. R.; Tidecks, R. *Phys. Rev. B* **2017**, *96*, 184521. doi:10.1103/PhysRevB.96.184521.

57. Klenov, N.; Khaydukov, Y.; Bakurskiy, S.; Morari, R.; Soloviev, I.; Boian, V.; Keller, T.; Kupriyanov, M.; Sidorenko, A.; Keimer, B. *Beilstein Journal of Nanotechnology* **2019**, *10* (1), 833–839.

58. Usadel, K. D. *Phys. Rev. Lett.* **1970**, *25*, 507–509. doi:10.1103/PhysRevLett.25.507.

59. Kuprianov, M. Y.; Lukichev, V. *Sov. Phys. JETP* **1988**, *67*, 1163.

60. Mironov, S.; Mel'nikov, A.; Buzdin, A. *Applied Physics Letters* **2018**, *113* (2), 022601.

61. Annunziata, A. J. *Single-photon detection, kinetic inductance, and non-equilibrium dynamics in niobium and niobium nitride superconducting nanowires*; Yale University, 2010.

62. Marychev, P.; Vodolazov, D. Y. *Journal of Physics: Condensed Matter* **2021**, *33* (38), 385301.

63. Kapran, O. M.; Morari, R.; Golod, T.; Borodianskyi, E. A.; Boian, V.; Prepelita, A.; Klenov, N.; Sidorenko, A. S.; Krasnov, V. M. *Beilstein journal of nanotechnology* **2021**, *12* (1), 913–923.